Original Article

Institution of MECHANICAL ENGINEERS
Journal of ENGINEERING MANUFACTURE

Proc IMechE Part B:
J Engineering Manufacture
2018, Vol. 232(14) 2592–2604

DOI: 10.1177/0954405417697349
journals.sagepub.com/home/pib
SAGE

Positioning variation modeling for aircraft panels assembly based on elastic deformation theory

Qing Wang[1,2,3], Renluan Hou[1,2,3], Jiangxiong Li[1,2,3], Yinglin Ke[1,2,3], Paul George Maropoulos[4] and Xianzhi Zhang[5]

Abstract

Dimensional variation in aircraft panel assembly is one of the most critical issues that affect the aerodynamic performance of aircraft, due to elastic deformation of parts during the positioning and clamping process. This article proposes an assembly deformation prediction model and a variation propagation model to predict the assembly variation of aircraft panels, and it derives consecutive three-dimensional deformation expressions which explicitly describe the nonlinear behavior of physical interaction occurring in compliant components assembly. An assembly deformation prediction model is derived from equations of statics of elastic beam to calculate the elastic deformation of panel component resulted from positioning error and clamping force. A variation propagation model is used to describe the relationship between local variations and overall assembly variations. Assembly variations of aircraft panels due to positioning error are obtained by solving differential equations of statics and operating spatial transformations of the coordinate. The calculated results show a good prediction of variation in the experiment. The proposed method provides a better understanding of the panel assembly process and creates an analytical foundation for further work on variation control and tolerance optimization.

Keywords

Aircraft panel assembly, positioning variation, elastic deformation theory, variation propagation model

Date received: 21 May 2016; accepted: 27 January 2017

Introduction

A large aircraft is commonly assembled by fuselage segments and wings, which are constructed by individual panels. Panel assembly is the first stage of the aircraft assembly, in which a skin has been riveted or bolted with longitudinal stiffeners (stringers) and circumferential stiffeners (frames). Each stringer–fame intersection is joined by small pieces called chips. The level of dimensional variation in panel assembly directly affects the final performance and capabilities of aircraft. However, it is difficult to predict and control the assembly variations of aircraft panels, since it is a semi-monocoque structure in large size, and the natural characteristics and assembly manners of panels often induce different degrees of deformation during assembly. Especially in panel assembly, positioning error and clamping force of stringers and frames are of severe effects to the dimensional variation of panels. It is essential to develop a mathematical model of panel assembly variation to describe these effects.

The analysis of assembly variation propagation is divided into two steps. The first step establishes an assembly model that simulates the assembly process to describe the interactions between parts and fixtures and the changes of product characteristics after assembly. The second step introduces the variations of the

[1]The State Key Laboratory of Fluid Power Transmission and Control, Zhejiang University, Hangzhou, China
[2]Key Laboratory of Advanced Manufacturing Technology of Zhejiang Province, Zhejiang University, Hangzhou, China
[3]Institute of Mechanical Engineering and Automation, College of Mechanical Engineering, Zhejiang University, Hangzhou, China
[4]Department of Mechanical Engineering, Aston University, Birmingham, UK
[5]School of Mechanical and Automotive Engineering, Kingston University, London, UK

Corresponding author:
Qing Wang, Institute of Mechanical Engineering and Automation, College of Mechanical Engineering, Zhejiang University, 38 Zheda Road, Hangzhou 310027, China.
Email: wqing@zju.edu.cn

individual components into the assembly model and uses the variation propagation model to estimate the dimensional change of the final product.

In the first step, some assembly models have been established in several major categories in recent industrial and academic research. Based on coordinate transformation theory, Chang and Gossard[1] proposed a geometric model ignoring components deformation, which can only be applied to the rigid assembly of components with the simple geometrical profile. Liu and Hu[2,3] presented a mechanical model to simplify assembly parts as one-dimensional (1D) cantilevered beams and derivate in-plane distortion formula of assembly joints with linear mechanics theories. A structural model proposed by Dahlstrom and Soderberg[4] is applied on early evaluation of conceptual assembly design based on a hierarchical product description and constraint decomposition. Contrarily, Cai et al.[5] presented digital panel assembly methodologies to predict assembly dimensions with operational assembly process simulation. A virtual assembly model was utilized by Vichare et al.[6] to integrate physical in-process measurement data into wing-box assembly variation analysis with computer-aided design (CAD) and finite element method (FEM) commercial software. The FEMs have been extensively utilized as the growing complexity of assembly simulation. To improve the efficiency of FEM analysis, Lin et al.[7] used the substructures of identical parts to simplify the deviation propagation model of aeronautical panel assembly, which is suitable for assembly model with numerous interchangeable parts.

The second step of assembly variations prediction is the variation propagation simulating phase. The traditional variation simulation methods include worst case analysis and root sum of squares which are overestimating variation spread. Subsequently, assembly variation models considering part deformation during the assembly process are paid more attention to analytical study. Method of influence coefficients (MIC)[8] adopted FEMs to construct sensitivity matrix that describes a linear relationship of input part variation and the output assembly variation. Principal component analysis (PCA)[9] extracted the deformation patterns from the production data by decomposing the component covariance into the individual contributions of several deformation patterns. Liao and Wang[10] applied wavelets transform to decompose assembly variations into different scale components and calculated the corresponding deformation of non-rigid assemblies using FEM. To solve the variation synthesis optimization problems, the statistical analysis and quality engineering methods are generally used, aiming to integrate the key production characters (KPCs) and key control characters (KCCs) to ensure the minimum assembly variation.[11] Bowman[12] utilized Monte Carlo simulation to select design tolerances for component dimensions of a mechanical assembly to minimize manufacturing cost. However, sample size has a major influence on the accuracy of Monte Carlo simulation. Wang[13] employed design of experiment (DOE) method to analyze the interactive relationship between edge's and rib's distortion. Moreover, some stochastic search methods were used to analyze variation propagation models and solve the tolerance synthesis problems with non-normal distribution, such as simulated annealing, genetic algorithms,[14] ant colony optimization algorithms and particle swarm optimization.[15] However, it is noted that such searching methods cannot guarantee global optima.

Meanwhile, the focus of variation analysis of the multi-station hierarchical assembly processes is the establishment of the relationship between the tolerances of process elements across multiple stages and the variation of the final product. Among the models of multi-station assembly variation propagation, the state space method[16,17] and stream of variation methodology[18] are explored in much greater depth due to their linear structure and the automatic handling of complicated stage-wise interaction. In aircraft assembly process, assembly variation is affected not only by positioning, clamping,[19] joining[2,3,13,20] and so on, but also by part distortion in manufacture.[21] Chantzis et al.,[21] D'Alvise et al.[22] and Sim[23] presented an industrial solution based on years of fundamental research to minimize part distortion due to residual stresses for machining of large monolithic components in aerospace industry. This solution would help reduce the impact of part distortion on assembly variation.

Most of the above-proposed mathematical models of assembly variation analysis utilized the linear combination of displacement of discrete KCCs to represent assembly variations of KPCs. Since the nonlinear behavior of the physical interaction between components and tooling is not taken into consideration in the simplified linear model, the calculated values distinctly vary from the actual assembly variations. Although FEM can simulate the nonlinear assembly process, the nonlinear relationship between input dimensional variation (before assembly) and output dimensional variation (after assembly) described by FEM is implicit, which makes nonlinear analytical mathematic efforts useless.[24] In summary, it is necessary to study a nonlinear model to predict variation propagation in the assembly process. Based on minimum potential energy principle, this article first presents a deformation prediction model to obtain the analytical solutions of the differential equations for deformation function with panel positioning variations. Second, the propagation relationships between the dimensional variations of differential elements and the part entity are established by introducing spatial transformations as an innovative point of this work. Finally, the calculated assembly variation propagation results with the proposed method are analyzed and compared with the simulation results using FEM and the measured variation data in experiments.

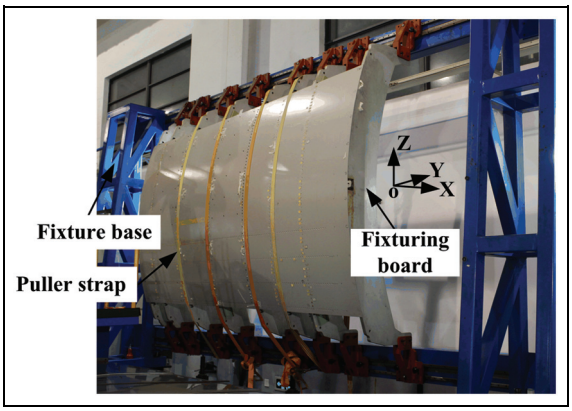

Figure 1. Panel assembly fixture.

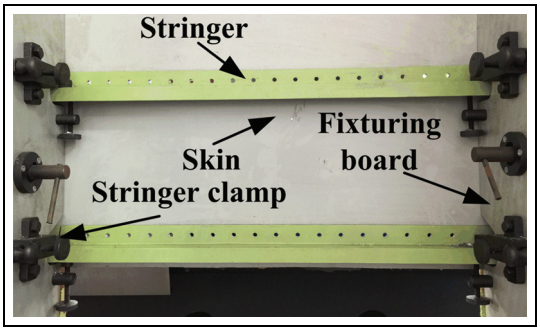

Figure 2. Stringer positioning element.

Deformation prediction model and variation propagation model

The assembly process of fuselage panel includes positioning, drilling, countersinking, sealing and riveting, in which the positioning accuracy of structural parts such as frames and stringers, directly affects the subsequent steps. Dimension accuracy of the panel chiefly depends on the positioning accuracy of frames and stringers rather than skin because of their stronger stiffness. Therefore, positioning variations of stringers are investigated in the following sections.

In the aircraft assembly, stringers, frames and skin shown in Figure 1 are assembled in a fixture and tacked together with temporary fasteners or fastened together with puller straps before being riveted together. The fixture is composed of fixture base, fixture boards which are used to locate the stringers and preserve the shape of skin, and puller straps. Clamping mechanisms fixed on the fixture board are utilized to position and clamp the stringers, as shown in Figure 2.

Deformation prediction model for stringer positioning assembly

The stringer is simplified into a beam since its cross-sectional width is much smaller than the length. When the stringer is positioned and clamped, the positional variation is simplified to the displacement of the anchor point to clarify how the variations of anchor points affect the stringer deformation. First, the stringer and positioning elements (as shown in Figure 2) are simplified in panel assembly fixture to analyze anchor point variations and stringer deformation. In Figure 3, nominal position of a stringer is shown in Figure 3(a); anchor point variation and stringer deformation are shown in Figure 3(b).

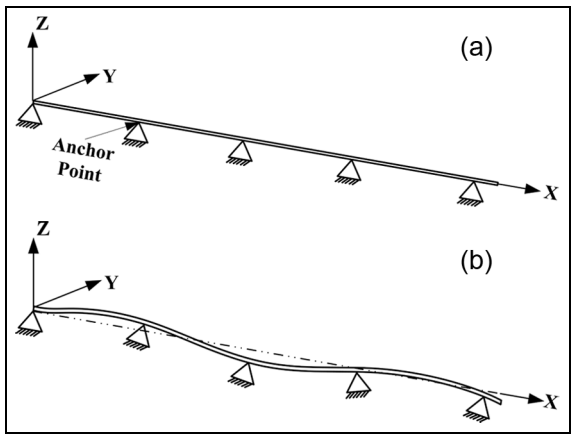

Figure 3. Mechanical simplification of the stringer and positioning element: (a) nominal position of a stringer and (b) anchor point variations and stringer deformation.

This article adopts the energy method to calculate deformation potential of the stringer caused by variation of anchor point. Based on energy conservation theory, deformation potential is irrelevant with the sequence of forces applied on the elastomer. Instead, it is totally determined by the eventual stress and deformation. Therefore, it can be assumed that the six independent quantities of stress and their corresponding deformation components simultaneously reach the final state. An overall strain energy density can be obtained by figuring out strain energy density of each component and then stacking them up. The work applied on each strain is deformation potential.

The local coordinate system is displayed in Figure 4. Axis x_1 of the stringer is the locus of the centers of inertia of the cross section. Axes x_2 and x_3 which are perpendicular to each other, lying in the cross-sectional plane, are shown in Figure 4. Displacement is $u_i = u_i(x_1),\ i = 1, 2, 3.$ u_i is the displacement in x_i-direction. Longitudinal displacement is u_1; lateral displacements are u_2, u_3. Since the cross area is quite small, it is assumed that the lateral displacements of the points on the same cross area are consistent, which means u_2 and u_3 are equal to deflection in two directions of x_2 and x_3 along the axis x_1

$$u_2(x_1, x_2, x_3) \approx u_2^{(0)}(x_1),\ u_3(x_1, x_2, x_3) \approx u_3^{(0)}(x_1) \qquad (1)$$

Rotation is $\omega_i = u_{3+i},\ i = 1, 2, 3,$ where ω_i is the angle rotating around axis x_i, and defined by

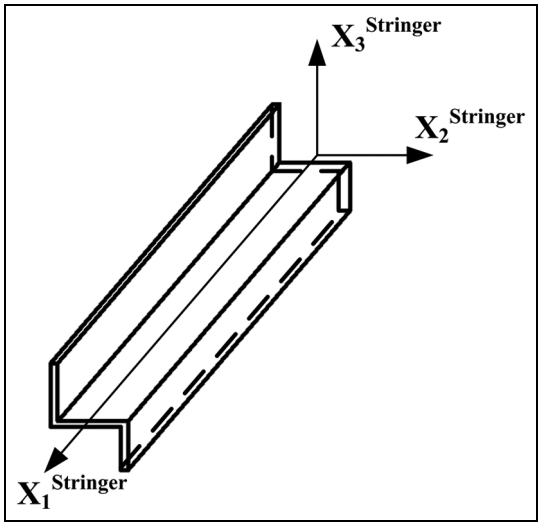

Figure 4. Local coordinate system.

$$\omega_1 = u_4,\ \omega_2 = -\frac{du_3}{dx_1},\ \omega_3 = \frac{du_2}{dx_1} \tag{2}$$

Strain energy separately caused by tension, bending moment, torque and shear force applying on the stringer is discussed below. For the convenience of calculation, components of stress and corresponding directions are defined in Figure 5. With tension applied, elongation of displacement u_1 in the direction of x_1 is positive strain, which is given by

$$\varepsilon_{11} = \varepsilon_{11}(u) = \frac{du_1}{dx_1} = u_1' \tag{3}$$

Since stringer deformation is elastic, based on Hooke's law, the internal force of cross section is calculated by

$$Q_1 = EA\varepsilon_{11}(u) = EAu_1' \tag{4}$$

Strain energy[25] occurring in the process of extension and contracting of the stringer is calculated by

$$\frac{1}{2}D_1(u,u) = \frac{1}{2}\int Q_1(u)\varepsilon_{11}(u)dx_1 = \frac{1}{2}\int EA\varepsilon_{11}^2(u)dx_1 \tag{5}$$

With bending moment applied, curvatures around axis x_2 and x_3 are, respectively, given by

$$K_2 = K_2(u) = \frac{d\omega_2}{dx_1} = -\frac{d^2u_3}{dx_1^2} = -u_3'' \tag{6}$$

$$K_3 = K_3(u) = \frac{d\omega_3}{dx_1} = \frac{d^2u_2}{dx_1^2} = u_2'' \tag{7}$$

For the bending moment, the following equations are deduced

$$M_2 = M_2(u) = EI_{22}K_2 + EI_{23}K_3 = -EI_{22}u_3'' + EI_{23}u_2'' \tag{8}$$

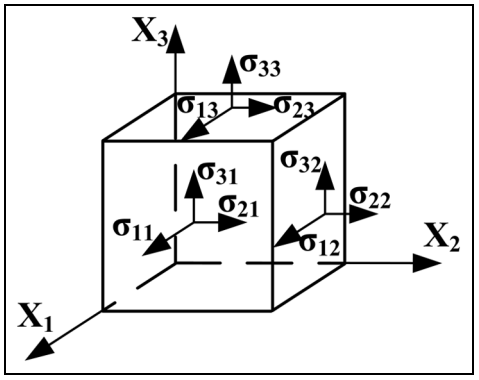

Figure 5. Directions of stress component.

$$M_3 = M_3(u) = EI_{32}K_2 + EI_{33}K_3 = -EI_{32}u_3'' + EI_{33}u_2'' \tag{9}$$

where EI_{ij} is the bending stiffness, I_{ij} is an inertia moment of the cross section. Furthermore, transversal shear forces generated by shear stress σ_{21} and σ_{31} on each cross section along axis x_1 are, respectively, given by

$$Q_2 = Q_2(u) = -\frac{dM_3(u)}{dx_1} = -M_3' = EI_{32}u_3^{(3)} - EI_{33}u_2^{(3)} \tag{10}$$

$$Q_3 = Q_3(u) = \frac{dM_2(u)}{dx_1} = M_2' = -EI_{22}u_3^{(3)} + EI_{23}u_2^{(3)} \tag{11}$$

Strain energy occurring in the process of stringer bending is calculated by

$$\begin{aligned}\frac{1}{2}D_{23}(u,u) &= \frac{1}{2}\int\sum_{i=2}^{3}M_i(u)K_i(u)dx_1 \\ &= \frac{1}{2}\int\sum_{i,j=2}^{3}EI_{ij}K_i(u)K_j(u)dx_1\end{aligned} \tag{12}$$

With torsion applied, rate of torsion and torque are calculated from the following equations

$$K_1 = K_1(u) = \frac{d\omega_1}{dx_1} = \frac{du_4}{dx_1} = u_4' \tag{13}$$

$$\begin{aligned}M_1 = M_1(u) &= \frac{E}{2(1+\nu)}JK_1 \\ &= GJK_1 = \frac{E}{2(1+\nu)}Ju_4' = \frac{E}{2(1+\nu)}J\omega_1'\end{aligned} \tag{14}$$

where ν is Poisson's ratio, G is the elastic shear modulus and J is the geometric torsional stiffness. Strain energy occurring in the process of stringer torsion is calculated by

$$\frac{1}{2}D_4(u,u) = \frac{1}{2}\int M_1(u)K_1(u)dx_1 = \frac{1}{2}\int GJK_1^2(u)dx_1 \tag{15}$$

Thus, total strain energy is given by

$$\frac{1}{2}D(u,u) = \frac{1}{2}[D_1(u,u) + D_{23}(u,u) + D_4(u,u)] \tag{16}$$

Strain energy functional in terms of the strain components is denoted as follows

$$D_1(u,v) = \int Q_1(u)\varepsilon_{11}(v)dx_1 = \int EA\varepsilon_{11}(u)\varepsilon_{11}(v)dx_1 \tag{17}$$

$$\begin{aligned} D_{23}(u,v) &= \int \sum_{i=2}^{3} M_i(u)K_i(v)dx_1 \\ &= \int \sum_{i,j=2}^{3} EI_{ij}K_i(u)K_j(v)dx_1 \end{aligned} \tag{18}$$

$$D_4(u,v) = \int M_1(u)K_1(v)dx_1 = \int GJK_1(u)K_1(v)dx_1 \tag{19}$$

Total strain energy functional is given by

$$D(u,v) = D_1(u,v) + D_{23}(u,v) + D_4(u,v) \tag{20}$$

Based on the formula of integration by parts and Green's theorem, the strain energy functional of extension or contracting stringer is written in the form

$$\begin{aligned} D_1(u,v) &= \int Q_1(u)\varepsilon_{11}(v)dx_1 = \int EA\varepsilon_{11}(u)\varepsilon_{11}(v)dx_1 \\ &= \int EAu'_1v'_1dx_1 = [EAu'_1v_1]_{\delta_1}^{\delta_2} - \int_{\delta_1}^{\delta_2}(EAu'_1)'v_1dx_1 \end{aligned} \tag{21}$$

where δ_i denotes the contour of the stringer bounding the whole region.

Strain energy functional of bending stringer is extended by

$$\begin{aligned} D_{23}(u,v) &= \int [M_2(u)K_2(v) + M_3(u)K_3(v)]dx_1 \\ &= \int \left[-M_2(u)v''_3 + M_3(u)v''_2\right]dx_1 \\ &= [M_3(u)v'_2]_{\delta_1}^{\delta_2} - \int_{\delta_1}^{\delta_2} M'_3(u)v'_2dx_1 - [M_2(u)v'_3]_{\delta_1}^{\delta_2} + \int_{\delta_1}^{\delta_2} M'_2(u)v'_3dx_1 \\ &= [M_3(u)v'_2 - M_2(u)v'_3 - M'_3(u)v_2 + M'_2(u)v_3]_{\delta_1}^{\delta_2} + \int_{\delta_1}^{\delta_2}\left[M''_3(u)v_2 - M''_2(u)v_3\right]dx_1 \\ &= [(-EI_{32}u''_3 + EI_{33}u''_2)v'_2 - (-EI_{22}u''_3 + EI_{23}u''_2)v'_3 - (-EI_{32}u^{(3)}_3 + EI_{33}u^{(3)}_2)v_2 \\ &\quad + (-EI_{22}u^{(3)}_3 + EI_{23}u^{(3)}_2)v_3]_{\delta_1}^{\delta_2} + \int_{\delta_1}^{\delta_2}[(-EI_{32}u^{(4)}_3 + EI_{33}u^{(4)}_2)v_2 - (-EI_{22}u^{(4)}_3 + EI_{23}u^{(4)}_2)v_3]dx_1 \end{aligned} \tag{22}$$

Strain energy functional of torsion stringer is written as

$$\begin{aligned} D_4(u,v) &= \int M_1(u)K_1(v)dx_1 \\ &= -\int_{\delta_1}^{\delta_2}[M'_1(u)v_4]dx_1 + [M_1(u)v_4]_{\delta_1}^{\delta_2} \end{aligned} \tag{23}$$

The force loaded on the stringer can be defined as $f_i = f_i(x_1),\ \ i = 1,2,3$. f_i is the linear force along the axis x_i, then the torque load is the linear force along the axis x_i which is denoted by $m_1 = m_1(x_1) = f_4(x_1)$. External work of tensile force, bending force and torsional force loaded on stringer are, respectively, given by

$$\begin{aligned} -F_1(v) &= -\int f_1v_1dx_1 = -\int_{\delta_1}^{\delta_2} f_1v_1dx_1 \\ &= -\int_{\delta_1}^{\delta_2} f_1v_1dx_1 - [f_1v_1]_{\delta_1} - [f_2v_2]_{\delta_2} \end{aligned} \tag{24}$$

$$\begin{aligned} -F_{23}(v) &= -\int (f_2v_2 + f_3v_3)dx_1 = -\int_{\delta_1}^{\delta_2}(f_2v_2 + f_3v_3)dx_1 \\ &= -\int_{\delta_1}^{\delta_2}(f_2v_2 + f_3v_3)dx_1 - [f_2v_2]_{\delta_1} - [f_3v_3]_{\delta_1} - [f_2v_2]_{\delta_2} - [f_3v_3]_{\delta_2} \\ &\quad - [f_5v_5]_{\delta_1} - [f_5v_5]_{\delta_2} - [f_6v_6]_{\delta_1} - [f_6v_6]_{\delta_2} \end{aligned} \tag{25}$$

$$\begin{aligned} -F_4(v) &= -\int m_1\omega_1dx_1 = -\int_{\delta_1}^{\delta_2} f_4v_4dx_1 \\ &= -\int_{\delta_1}^{\delta_2} f_4v_4dx_1 - [f_4v_4]_{\delta_1} - [f_4v_4]_{\delta_2} \end{aligned} \tag{26}$$

The potential energy[26] of the system is equal to the difference between the strain energy and the work of external forces, which can be obtained by

$$J(u) = \frac{1}{2}D(u,u) - F(u) \tag{27}$$

Based on the principle of minimum potential energy of the system, the stationary value of functional $J(u)$ in the equilibrium position is a minimum, which is equivalent to $D(u, v) - F(v) = 0$ for all v, namely

$$x_1 = \delta_x : \begin{cases} u_i = \bar{u}_i^{\delta_x} \\ \omega_i = \bar{\omega}_i^{\delta_x} \end{cases}, \quad i = 1, 2, 3 \tag{34}$$

$$\begin{aligned} D(u, v) - F(v) &= D_1(u, v) + D_{23}(u, v) + D_4(u, v) - F_1(v) - F_{23}(v) - F_4(v) \\ &= -\int_{\delta_1}^{\delta_2} [Q_1(u) + f_1] v_1 dx_1 + [Q_1(u) - f_1]_{\delta_2}[v_1]_{\delta_2} - [Q_1(u) + f_1]_{\delta_1}[v_1]_{\delta_1} \\ &\quad + \int_{\delta_1}^{\delta_2} [M_3''(u) - f_2] v_2 dx_1 - \int_{\delta_1}^{\delta_2} [M_2''(u) + f_3] v_3 dx_1 \\ &\quad + [M_3(u) - f_6]_{\delta_2}[v_6]_{\delta_2} + [M_2(u) - f_5]_{\delta_2}[v_5]_{\delta_2} - [M'_3(u) + f_2]_{\delta_2}[v_2]_{\delta_2} \\ &\quad + [M'_2(u) - f_3]_{\delta_2}[v_3]_{\delta_2} - [M_3(u) + f_6]_{\delta_1}[v_6]_{\delta_1} - [M_2(u) + f_5]_{\delta_1}[v_5]_{\delta_1} \\ &\quad + [M'_3(u) - f_2]_{\delta_1}[v_2]_{\delta_1} - [M'_2(u) + f_3]_{\delta_1}[v_3]_{\delta_1} \\ &\quad - \int_{\delta_1}^{\delta_2} [M'_1(u) + f_4] v_4 dx_1 + [M_1(u) - f_4]_{\delta_2}[v_4]_{\delta_2} - [M_1(u) + f_4]_{\delta_1}[v_4]_{\delta_1} \\ &= 0 \end{aligned} \tag{28}$$

When the stringer is free from geometric constraint, based on variation principle, u in an equilibrium state makes the equation true for all v (including v_i), which is equivalent to the equilibrium equation with the expression in brackets of the above equation equal to 0. All equilibrium equations are listed as follows

$$\delta_1 < x_1 < \delta_2 : -\frac{dQ_i(u)}{dx_1} = f_i \quad i = 1, 2, 3 \tag{29}$$

$$-\frac{dM_1(u)}{dx_1} = f_4 \tag{30}$$

which is

$$\delta_1 < x_1 < \delta_2 : \begin{cases} -EAu_1'' = f_1 \\ -EI_{32}u_3^{(4)} + EI_{33}u_2^{(4)} = f_2 \\ EI_{22}u_3^{(4)} - EI_{23}u_2^{(4)} = f_3 \\ -\dfrac{E}{2(1+\nu)} J\omega_1'' = m_1 \end{cases} \tag{31}$$

$$x_1 = \delta_1 : \begin{cases} -Q_i(u) = [f_i]_{\delta_1} \\ -M_i(u) = [f_{3+i}]_{\delta_1} \end{cases} \quad i = 1, 2, 3 \tag{32}$$

$$x_1 = \delta_2 : \begin{cases} -Q_i(u) = [f_i]_{\delta_2} \\ -M_i(u) = [f_{3+i}]_{\delta_2} \end{cases} \quad i = 1, 2, 3 \tag{33}$$

The above formulae with $x_1 = \delta_1$, $x_1 = \delta_2$ satisfies boundary compatibility conditions and also natural boundary condition, indicating the balance of shearing force, tension, bending moment and torque at the endpoint. When the boundary of stringer is applied with any known generalized displacement u_i, replace equations of load f_i that have the same subscript. Imposed boundary conditions is as follows

The function expression of stringer deformation $u_i(x_1)$ $(i = 1, 2, 3, 4)$ can be solved by simultaneous equations above. Furthermore, the relationship of assembly variations and anchor point variations can be obtained with a concrete function expression.

Propagation model of variation resulted from assembly deformation

Assembly variation indicates the offset that a part's actual assembled position deviates from designed assembly specification or its nominal position required in each assembly process. Moreover, the variations of the point on axis x_1 of the stringer due to positioning variation is denoted by

$$\Delta u_i(x_1) = u_i(x_1) - {}^0u_i(x_1) \quad (i = 1, 2, 3) \tag{35}$$

where $u_i(x_1)$ $(i = 1, 2, 3)$ are coordinate values for the actual positions of the points on axis x_1 of the positioned stringer. ${}^0u_i(x_1)$ $(i = 1, 2, 3)$ are coordinate values for their nominal positions. Thus, ${}^0u_i(x_1) = 0$ $(i = 1, 2, 3)$ can be obtained.

When the stringer is discretized, as shown in Figure 6, coordinate system $\{{}^0O\}$ represents the nominal position of stringer while coordinate system $\{O\}$ represents the actual position of assembled stringer. Point ${}^0O$ is the center of inertia of the cross section and the principal directions of coordinate system $\{{}^0O\}$ are ${}^0X_1$, ${}^0X_2$, and ${}^0X_3$, parallel to the axes x_1, x_2, and x_3 as known. When written in terms of coordinate system $\{O\}$, they are called as X_1, X_2, and X_3. The displacement of any point ${}^0P$ on the cross section of stringer is described by vector in system $\{{}^0O\}$, which can be calculated by

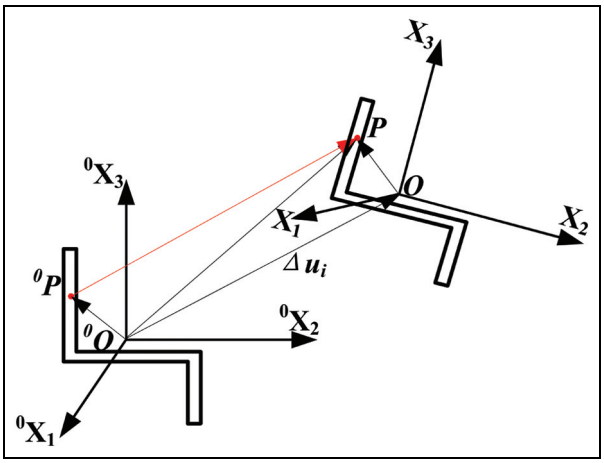

Figure 6. Coordinate transformation of anchor points on the same cross section of stringer.

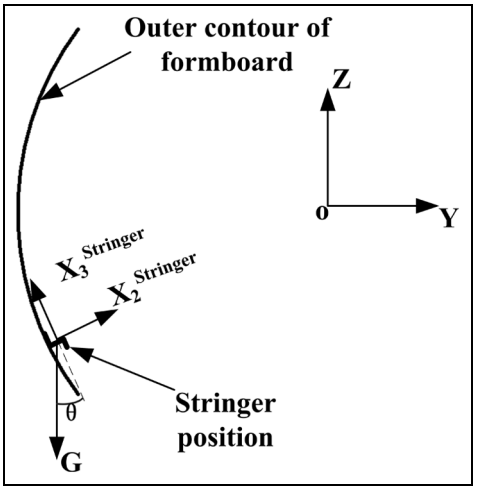

Figure 7. Position and direction of stringer in assembly process.

$$
\begin{aligned}
\overline{{}^0PP} &= \overline{{}^0OP} - \overline{{}^0O{}^0P} \\
&= {}^0\mathbf{R}\cdot\overline{OP} + \overline{{}^0OO} - \overline{{}^0O{}^0P} \\
&= {}^0\mathbf{R}\cdot\overline{{}^0O{}^0P} - \overline{{}^0O{}^0P} + \overline{{}^0OO} \\
&= ({}^0\mathbf{R}-\mathbf{E})\cdot\left[{}^0x_1^P - {}^0x_1^O \quad {}^0x_2^P - {}^0x_2^O \quad {}^0x_3^P - {}^0x_3^O\right]^T + \Delta\mathbf{u_i} \\
&= ({}^0\mathbf{R}-\mathbf{E})\cdot\left[{}^0x_1^P \quad {}^0x_2^P \quad {}^0x_3^P\right]^T + [\Delta u_1 \quad \Delta u_2 \quad \Delta u_3]^T
\end{aligned}
\tag{36}
$$

where the rotation matrix describes $\{O\}$ relative to $\{{}^0O\}$

$$
{}^0\mathbf{R}(\omega_1,\omega_2,\omega_3) = \begin{bmatrix} c\omega_3\cdot c\omega_2 & c\omega_3\cdot s\omega_2\cdot s\omega_1 - s\omega_3\cdot c\omega_1 & c\omega_3\cdot s\omega_2\cdot c\omega_1 + s\omega_3\cdot s\omega_1 \\ s\omega_3\cdot c\omega_2 & s\omega_3\cdot s\omega_2\cdot s\omega_1 + c\omega_3\cdot c\omega_1 & s\omega_3\cdot s\omega_2\cdot c\omega_1 - c\omega_3\cdot s\omega_1 \\ -s\omega_2 & c\omega_2\cdot s\omega_1 & c\omega_2\cdot c\omega_1 \end{bmatrix}
\tag{37}
$$

where $c\omega_i = \cos\omega_i, s\omega_i = \sin\omega_i,\ i = 1,2,3$. Thereby, when the stringer is clamped and positioned, a model for propagating variation of point ${}^0O$ (the center of inertia of the cross section) to variation of point ${}^0P$ (any point on the same cross section of stringer) is given by

$$
\mathbf{\Delta u_i^P} = ({}^0\mathbf{R}-\mathbf{E})\cdot\left[{}^0x_1^P \quad {}^0x_2^P \quad {}^0x_3^P\right]^T + \mathbf{\Delta u_i^0},\ (i=1,2,3)
\tag{38}
$$

where $\left[{}^0x_1^P \quad {}^0x_2^P \quad {}^0x_3^P\right]^T$ is the position vector of point ${}^0P$ in system $\{{}^0O\}$.

Case study of stringer positioning deformation and finite element simulation

Case study: theoretical calculation of stringer positioning deformation

The angle between the direction of gravity and the normal direction of the locating surface for the stringer, θ, is shown in Figure 7. Figure 8 shows the sectional dimension of the stringer. Other parameters of the stringers are presented in Tables 1 and 2.

The parameters are substituted into the equilibrium equation (31)

$$
10 < x_1 < 485: \begin{cases} -EAu_1'' = f_1 \\ -EI_{32}u_3^{(4)} + EI_{33}u_2^{(4)} = f_2 \\ EI_{22}u_3^{(4)} - EI_{23}u_2^{(4)} = f_3 \\ -\frac{E}{2(1+\nu)}J\omega_1'' = m_1 \end{cases}
$$

where $I_{32} = I_{23} = 1.403\times10^4\text{mm}^4$, $I_{33} = 2.342\times10^4\text{mm}^4$, and $I_{22} = 1.427\times10^4\text{mm}^4$ which are calculated based on the sectional dimension of the stringer shown in Figure 8. The results of equations are $u_2^{(4)} = constant, u_3^{(4)} = constant$. Thus, the displacements are assumed to be given by $u_i = a_ix_1^4 + b_ix_1^3 + c_ix_1^2 + d_ix_1 + e_i, i = 2,3$. Similar to the case of the other

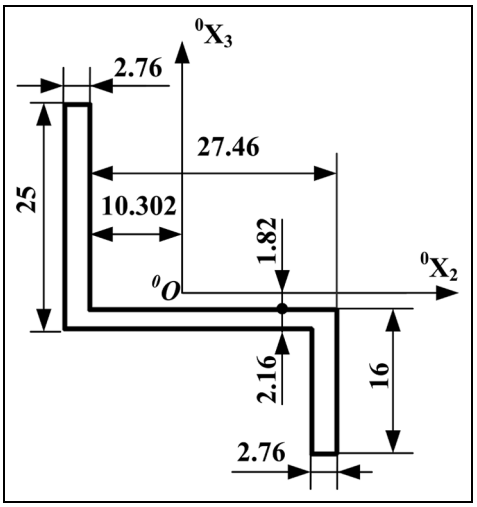

Figure 8. Sectional dimension of the stringer.

Table 1. Boundary conditions of theoretical model.

Variable	x_1 (mm)	$u_1(x_1)$ (mm)	$\omega_1(x_1)$ (rad)	$u_2(x_1)$ (mm)	$\omega_2(x_1)$ (rad)	$u_3(x_1)$ (mm)	$\omega_3(x_1)$ (rad)
δ_1	10	0	0	0	0	0	0
δ_2	485	0.458	−0.0897	−1.856	0	−2.439	−0.0437

Table 2. Physical and mechanical property parameters of the materials.

Part	Material	Density, ρ (g cm^{-3})	Cross-sectional area, A (mm^2)	Young's modulus, E (GPa)	Poisson's ratio, ν
Stringer	7050-T7651	2.83	166.5	72	0.33

Table 3. Calculated values of coefficients of the function expressions.

Coefficient	a_i	b_i	c_i	d_i	e_i
$i=1$				9.641×10^{-4}	-9.641×10^{-3}
$i=2$	-3.477×10^{-13}	-1.588×10^{-7}	7.205×10^{-5}	-1.393×10^{-3}	6.8875×10^{-3}
$i=3$	-5.189×10^{-13}	4.603×10^{-8}	-3.393×10^{-5}	6.6476×10^{-4}	-3.301×10^{-3}
$i=4$				-1.8884×10^{-4}	1.8884×10^{-3}

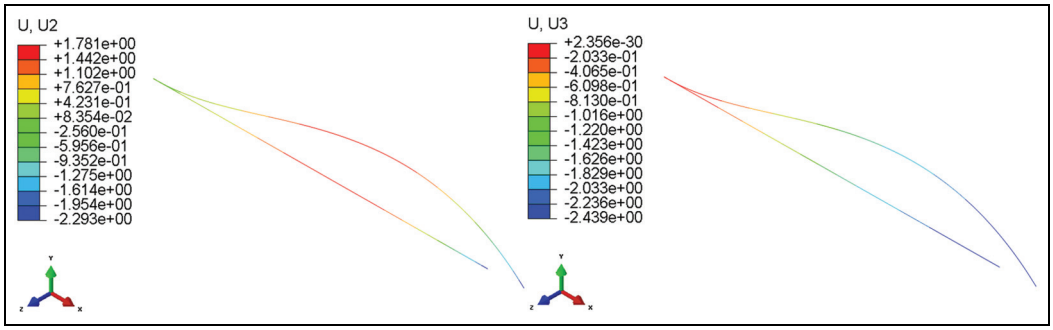

Figure 9. FE results of beam deformation.

displacement and rotation, they are expressed by $u_i = d_i x_1 + e_i, i = 1,4$, in terms of their constant second derivative which is 0, namely $u_1^{(2)} = 0, u_4^{(2)} = 0$. Values of coefficients of the function expressions are calculated and shown in Table 3.

Finite element simulation

Finite element (FE) model of a lateral fuselage panel component stringer is created using Abaqus® CAE as the pre-processor. The FE analysis (FEA) is carried out using the general purpose FEA package Abaqus Standard. Solid elements are adapted to general models. Since the obtained result of displacement cannot directly show the rotation of stringer deformation with torsion applied, so beam elements are required for stringer modeling to obtain rotation displacements at each point of stringer around the axis x_1. B31 elements are adopted to mesh the grids of stringer. The material parameters are shown in Table 2. Applied displacement boundary conditions are presented in Table 1 and gravity is also included in the model. FE results of beam deformation caused by variations of anchor point and gravity are shown in Figure 9.

Comparisons between results from the proposed theoretical model calculation and Abaqus® simulation are demonstrated in Figure 10. The corresponding variables u_2, u_3, ω_2 and ω_3 are the polynomial functions of the independent variable x_1, while the relationships between u_1, ω_1 and x_1 are linear. It is clear that the results of theoretical calculation and FEA are consistent.

Experimental verification

Measurement of the stringer deformation

The stringer is positioned with a dedicated fixture for positioning and clamping, with a distance of 475 mm between the two clamping elements, as illustrated in Figure 2. Leica AT901-LR® laser tracker is adopted to

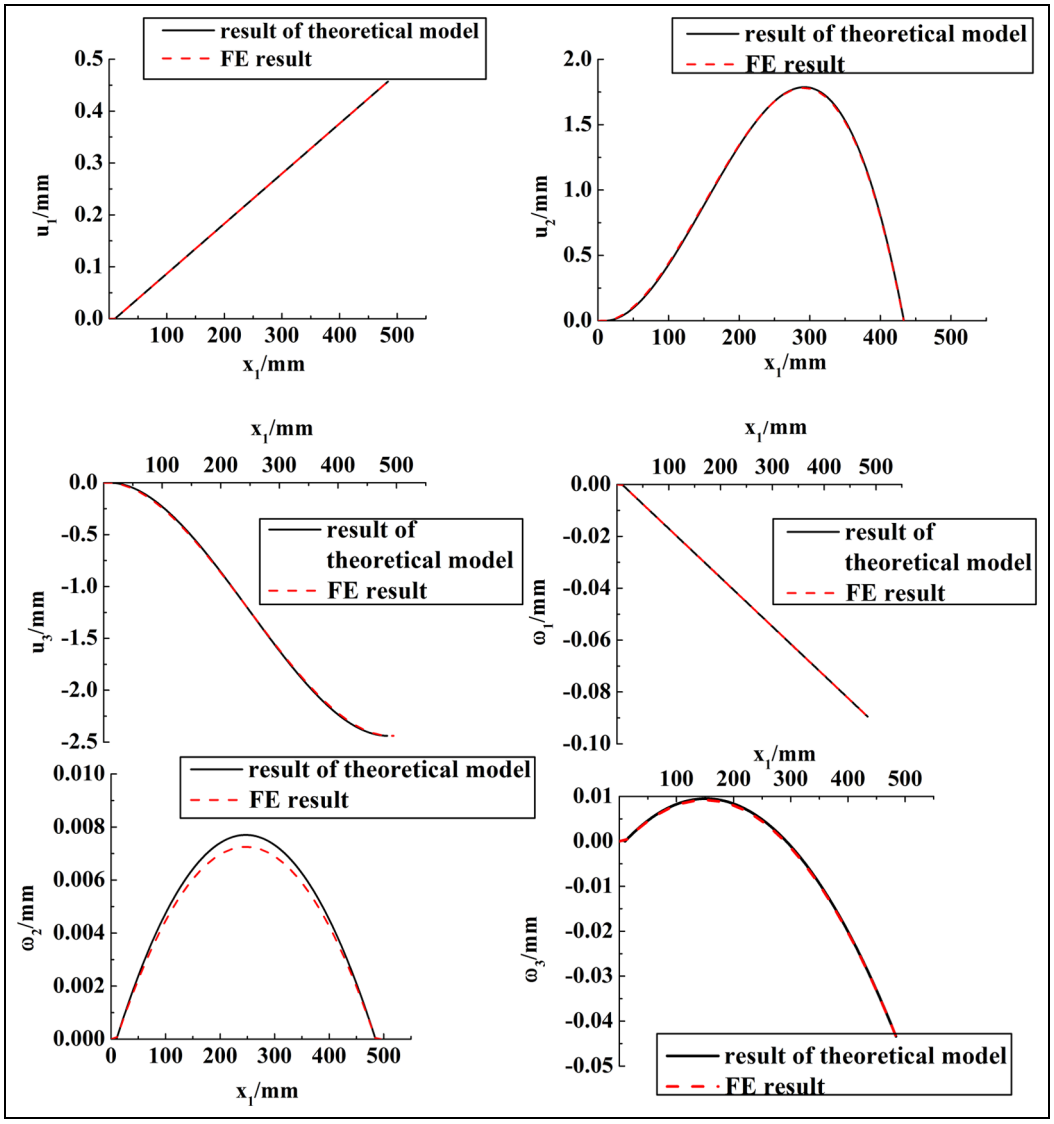

Figure 10. Comparison between results from theoretical model calculation and Abaqus® simulation.

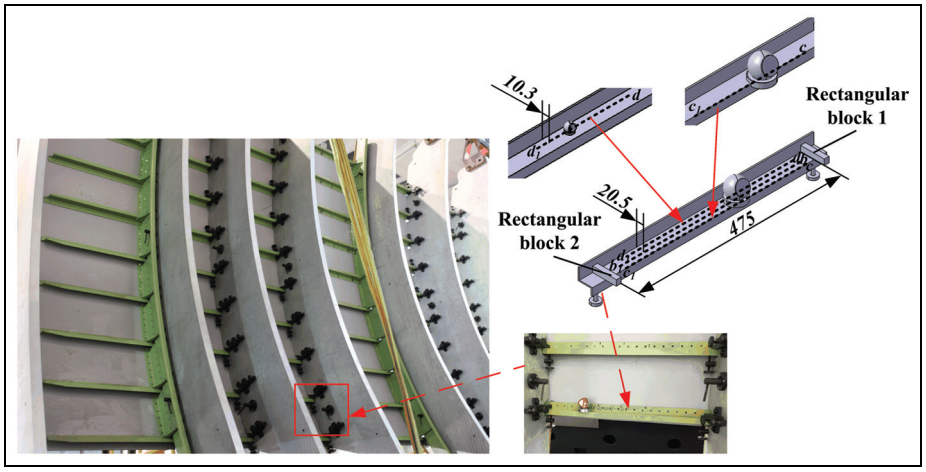

Figure 11. The location of surface points of stringer to be measured.

Table 4. Input values of variations in single and multi-factor experiments.

Constraints	Δu_1 (mm)	Δu_2 (mm)	Δu_3 (mm)	$\Delta\omega_1$ (rad)	$\Delta\omega_2$ (rad)	$\Delta\omega_3$ (rad)
I	0	0	−1.68	0	0	0
II	0	−2	0	0	0	0
III	0	2	0	0	0	0
IV	0.195	−0.952	0	0	0	−0.0187
V	0.458	−1.856	−2.439	−0.0897	0	−0.0437

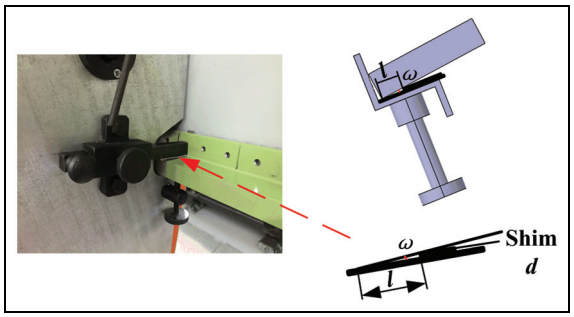

Figure 12. Methods and rotation angles applied to create variations in stringer assembly.

measure the surface of the stringer deformation arising in assembly. Displacements of all points and positions measured in the experiments are shown in Figure 11. The edge reflector holder and the shankless reflector holder are, respectively, allocated on the edge and the offset line of the edge to measure the coordinate values of all points.

Constraint displacements of Δu_1, Δu_2, Δu_3 and rotation angles of $\Delta\omega_1$, $\Delta\omega_2$, $\Delta\omega_3$ are applied to the clamped location by adding shims between clamping element rectangular block 2 and stringer surface. As shown in Figure 12, rotation angle ω is calculated by

$$\omega = \arctan\left(\frac{d}{l}\right) \tag{39}$$

Constraints of displacements and rotation angles adopted in the experiments are listed in Table 4.

Applications of boundary conditions in the experiments are shown in Figure 13.

As a benchmark, the nominal coordinate system of the stringer serves as an initial position in the actual coordinate system. Since this article takes no account of manufacturing errors, we have ${}^0u_i(x_1) = 0 \ (i = 1, 2, 3)$. Variation values of the central axis of inertia of the stringer cross section are displacement values of their deformation. With the use of the model, which propagates variations of the central axis of inertia of the cross sections to the variations of all points on the stringer, theoretical variation values of points on the stringer are available.

Results and discussion

Comparisons between measured values of u_1, u_2, u_3 (actual variations) on the offset lines of bb_1, cc_1, dd_1 and calculated theoretical variation values are made as shown in Figure 14.

The first three experiments are single factor experiments, of which varying parameters are, respectively, the constraints of displacements Δu_3 and Δu_2, aside from the constraints of rotation angles. As shown in Figure 14(a), the corresponding variable u_3 is approximately the polynomial function of the independent variable x_1. The relative deformation of different parts of the entity does not change obviously with the

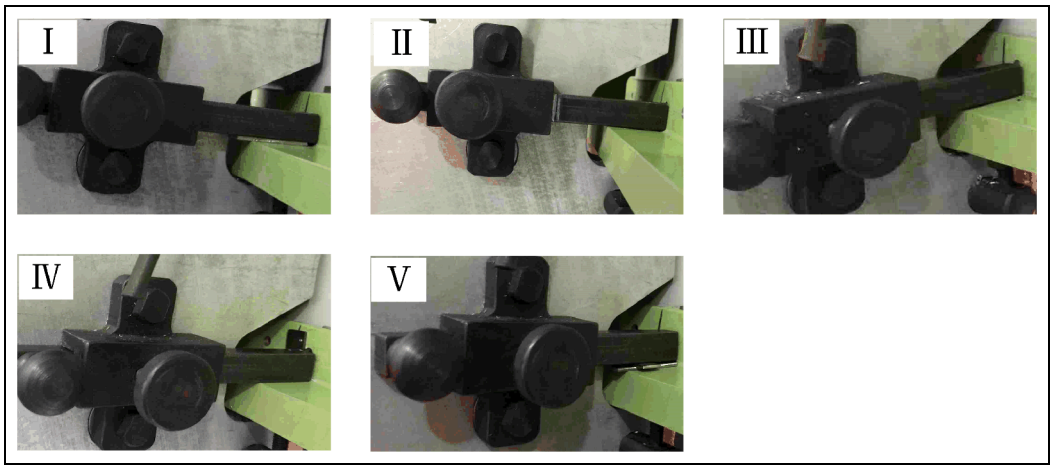

Figure 13. Applications of boundary conditions in the experiments.

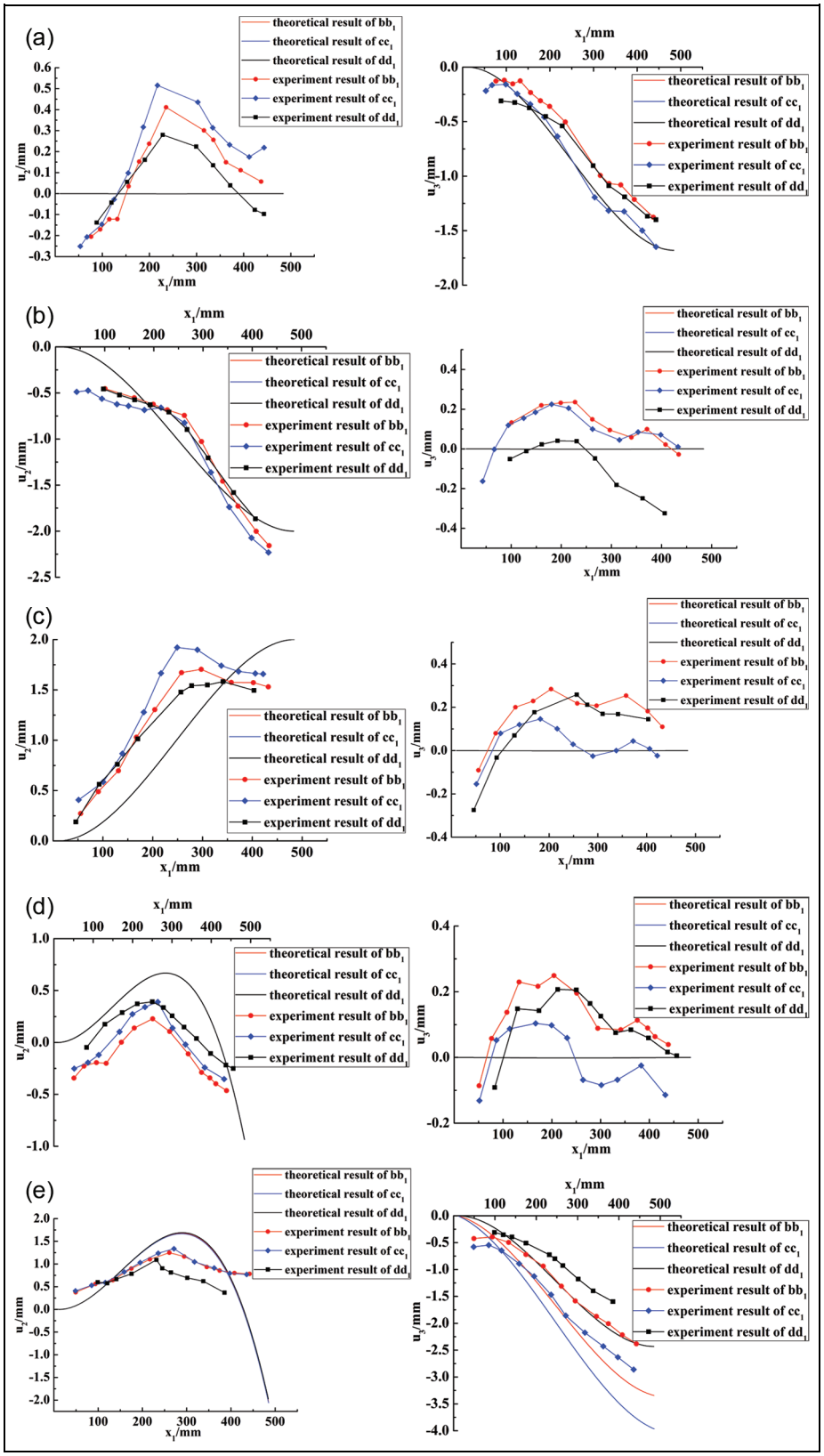

Figure 14. Calculated theoretical variation values and measured values (actual variations) of the offset lines bb_1, cc_1, dd_1: (a) theoretical and measured values of the position variations of bb_1, cc_1, dd_1 with the change of x_1 on the direction of x_2, x_3 in experiment I, (b) theoretical and measured values of the position variations of bb_1, cc_1, dd_1 with the change of x_1 on the direction of x_2, x_3 in experiment II, (c) theoretical and measured values of the position variations of bb_1, cc_1, dd_1 with the change of x_1 on the direction of x_2, x_3 in experiment III, (d) theoretical and measured values of the position variations of bb_1, cc_1, dd_1 with the change of x_1 on the direction of x_2, x_3 in experiment IV and (e) theoretical and measured values of the position variations of bb_1, cc_1, dd_1 with the change of x_1 on the direction of x_2, x_3 in experiment V.

Table 5. Statistical analysis results for experiment V.

		u_2	u_3
u_2	Pearson correlation	1	0.296
	Sig. (two-tailed)		0.377
	N	11	11
u_3	Pearson correlation	0.296	1
	Sig. (two-tailed)	0.377	
	N	11	11

Table 6. Means and standard deviations of the variations between experimental and theoretical values of dd_1 in the experiment.

Conditions	Means of variations (mm)		Standard deviations of variations (mm)	
	$\overline{\delta_{u_2}}$	$\overline{\delta_{u_3}}$	σ_{u_2}	σ_{u_3}
I	0.0549065	0.1118076	0.136257	0.147843
II	0.014618	−0.08415	0.16724	0.125298
III	0.234211	0.099978	0.252261	0.153608
IV	−0.215753	0.095336	0.181135	0.085481
V	−0.355435	0.282771	0.380336	0.206827

location of the measured point. The functions of x_1, which are u_2 in experiment II and u_3 in experiment I, have the same tendency and has negative correlation with u_2 in experiment III, as shown in Figure 14(b) and (c). Furthermore, u_2 in experiments II and III are only determined by Δu_2. In experiment IV, both the constraints of displacements and rotation angles are adopted. The curvature of stringer changes greatly with the increased bending moment on the boundary, as shown in Figure 14(d). Compared with that in experiment I, however, u_3, the x_3-direction deformations of different parts of the stringer in experiment V, changes significantly with the locations of the measured points, which is due to the different values of $({}^0\mathbf{R} - \mathrm{E}) \cdot [\,{}^0x_1^P \quad {}^0x_2^P \quad {}^0x_3^P\,]^T$ in equation (38) for different experiments.

From u_2, u_3, the actual values of dd_1's variations on the direction of x_2, x_3, as shown in Figure 14(a)–(d), it can be seen that u_2, x_2-direction deformations of each point on the stringer, is exclusively determined by Δu_2 and $\Delta\omega_3$, uncorrelated with deformations on the other two coordinate directions. In the statistical analysis of actually measured values of dd_1 in multi-factor experiment V, as seen in Table 5, the result Sig. > 0.1 indicates u_2 and u_3 are uncorrelated. Therefore, basic hypotheses of the proposed method in section "Deformation prediction model for stringer positioning assembly," have been proven consistent with practice. Because of the random error occurs in the experiment process, a few actually measured data deviate from theoretical values which are zero as shown in Figure 14. According to means and standard deviations of the variations between experimental and theoretical values of dd_1, as listed in Table 6, combining with the simulation result in previous sections, it can be concluded that theoretical variation model is consistent with simulation result, confirming to the tendency of experimental values and applicable to engineering purpose. It can also be derived that theoretical result calculated by variation propagation model is consistent with actual measurement from comparison among actually measured values on multiple positions of bb_1, cc_1, dd_1.

Conclusion

Dimensional variation caused by deformation of the large component is a major problem for aircraft industry. This article analyzes the deformation caused by positioning variation based on elasticity theory of the principle of minimum potential energy and spatial transformations of coordinate. A theoretical model for predicting deformation of compliant part and a variation propagation model for determining the relationship between local variations and the whole assembly variations are presented. Main conclusions are as follows:

1. Compared with the measured values of the points on the surface of the deformed stringer in the positioning and clamping process and the FE simulation analysis results, the proposed deformation prediction model and variation propagation model have been proven accurate and the proposed method satisfies the practical application.
2. The nonlinear relationships between anchor point variation and assembly deformation are influenced by boundary conditions, including the displacements and rotation angles of the anchor points, and the relative locations of the different deformation parts of the entity.

The study of stringer assembly deformation caused by variation arising in the positioning and clamping process is a preliminary to panel assembly variation research. To meet with design requirement, variations present in the joining assembly of panel components including stringer, frame and skin need further investigation. Calculation results derived from the proposed theoretical model for predicting stringer deformation can be used as input conditions in the subsequent study of panel assembly variation and can also provide a basis for error sources investigation and mechanism study on how the assembly technology influents the assembly quality.

Declaration of conflicting interests

The author(s) declared no potential conflicts of interest with respect to the research, authorship and/or publication of this article.

Funding

The author(s) disclosed receipt of the following financial support for the research, authorship, and/or publication of this article: This work was supported by the National Natural Science Foundation of China (grant number 51375442).

References

1. Chang MH and Gossard DC. Modeling the assembly of compliant, non-ideal parts. *Comput Aided Design* 1997; 29: 701–708.
2. Liu SC and Hu SJ. An offset finite-element model and its applications in predicting sheet-metal assembly variation. *Int J Mach Tool Manu* 1995; 35: 1545–1557.
3. Liu SC, Hu SJ and Woo TC. Tolerance analysis for sheet metal assemblies. *J Mech Des: T ASME* 1996; 118: 62–67.
4. Dahlstrom S and Soderberg R. Towards a method for early evaluations of sheet metal assemblies. In: Bourdet P and Mathieu L (eds) *Geometric product specification and verification: integration of functionality*. Dordrecht: Springer, 2003, pp.275–286.
5. Cai WW, Hsieh CC, Long YF, et al. Digital panel assembly methodologies and applications for compliant sheet components. *J Manuf Sci E: T ASME* 2006; 128: 270–279.
6. Vichare P, Martin O and Jamshidi J. Dimensional management for aerospace assemblies: framework implementation with case-based scenarios for simulation and measurement of in-process assembly variations. *Int J Adv Manuf Tech* 2014; 70: 215–225.
7. Lin J, Jin S, Zheng C, et al. Compliant assembly variation analysis of aeronautical panels using unified substructures with consideration of identical parts. *Comput Aided Design* 2014; 57: 29–40.
8. Liu SC and Hu SJ. Variation simulation for deformable sheet metal assemblies using finite element methods. *J Manuf Sci E: T ASME* 1997; 119: 368–374.
9. Camelio JA, Hu SJ and Marin SP. Compliant assembly variation analysis using component geometric covariance. *J Manuf Sci E: T ASME* 2004; 126: 355–360.
10. Liao XY and Wang GG. Wavelets-based method for variation analysis of non-rigid assemblies. *Int J Mach Tool Manu* 2005; 45: 1551–1559.
11. Karmakar S and Maiti J. A review on dimensional tolerance synthesis: paradigm shift from product to process. *Assembly Autom* 2012; 32: 373–388.
12. Bowman RA. Efficient gradient-based tolerance optimization using Monte Carlo simulation. *J Manuf Sci E: T ASME* 2009; 131: 337–346.
13. Wang H. Deformation analysis in horizontal stabilizer assembly using FEA modeling and multilevel analysis. *J Aerospace Eng*. Epub ahead of print 26 June 2014. DOI: 10.1061/(ASCE)as.1943-5525.0000385.
14. Abedini V, Shakeri M, Siahmargouei MH, et al. Analysis of the influence of machining fixture layout on the workpiece's dimensional accuracy using genetic algorithm. *Proc IMechE, Part B: J Engineering Manufacture* 2014; 228: 1409–1418.
15. Liu P, Li Y, Zhang KF, et al. Based on region division setup planning for sheet metal assembly in aviation industry. *Proc IMechE, Part B: J Engineering Manufacture* 2013; 227: 153–161.
16. Ding Y, Shi JJ and Ceglarek D. Diagnosability analysis of multi-station manufacturing processes. *J Dyn Syst: T ASME* 2002; 124: 1–13.
17. Liu CH, Jin S, Lai XM, et al. Dimensional variation stream modeling of investment casting process based on state space method. *Proc IMechE, Part B: J Engineering Manufacture* 2015; 229: 463–474.
18. Ceglarek D and Prakash PKS. Enhanced piecewise least squares approach for diagnosis of ill-conditioned multistation assembly with compliant parts. *Proc IMechE, Part B: J Engineering Manufacture* 2012; 226: 485–502.
19. Bi YB, Yan WM and Ke YL. Multi load-transmitting device based support layout optimization for large fuselage panels in digital assembly. *Proc IMechE, Part C: J Mechanical Engineering Science* 2015; 229: 1792–1804.
20. Cheng L, Wang Q, Li J, et al. Variation modeling for fuselage structures in large aircraft digital assembly. *Assembly Autom* 2015; 35: 172–182.
21. Chantzis D, Van-der-Veen S, Zettler J, et al. An industrial workflow to minimize part distortion for machining of large monolithic components in aerospace industry. *Proced CIRP* 2013; 8: 281–286.
22. D'Alvise L, Chantzis D, Schoinochoritis B, et al. Modelling of part distortion due to residual stresses relaxation: an aeronautical case study. *Proced CIRP* 2015; 31: 447–452.
23. Sim WM. Residual stress engineering in manufacture of aerospace structural parts, 2012, http://www.transport-research.info/sites/default/files/project/documents/20121115_114058_91510_Paper_IDE_2011.pdf
24. Xie K. *Analysis, prediction and control of variation propagation in non-linear sheet metal assembly processes*. PhD Thesis, Michigan Technological University, Houghton, MI, 2009.
25. Hetnarski RB and Ignaczak J. *The mathematical theory of elasticity*. 2nd ed. Boca Raton, FL: CRC Press, 2011, pp.151–155.
26. Lurie AI. *Theory of elasticity*. Berlin: Springer, 2005, pp.180–183.